J|A|C|S ARTICLES

Published on Web 01/26/2009

Structures and Aggregation of the Methylamine−Borane Molecules, $Me_nH_{3-n}N\cdot BH_3$ ($n = 1-3$), Studied by X-ray Diffraction, Gas-Phase Electron Diffraction, and Quantum Chemical Calculations

Simon Aldridge,[†] Anthony J. Downs,*[,†] Christina Y. Tang,[†] Simon Parsons,*[,‡] Michael C. Clarke,[‡] Russell D. L. Johnstone,[‡] Heather E. Robertson,[‡] David W. H. Rankin,*[,‡] and Derek A. Wann[‡]

Inorganic Chemistry Laboratory, University of Oxford, South Parks Road, Oxford OX1 3QR, U.K., and School of Chemistry, University of Edinburgh, West Mains Road, Edinburgh EH9 3JJ, U.K.

Received September 25, 2008; E-mail: tony.downs@chem.ox.ac.uk; s.parsons@ed.ac.uk; d.w.h.rankin@ed.ac.uk

Abstract: The structures of the molecules methylamine−borane, $MeH_2N\cdot BH_3$, and dimethylamine−borane, $Me_2HN\cdot BH_3$, have been investigated by gas-phase electron diffraction (GED) and quantum chemical calculations. The crystal structures have also been determined for methylamine−, dimethylamine−, and trimethylamine−borane, $Me_nH_{3-n}N\cdot BH_3$ ($n = 1-3$); these are noteworthy for what they reveal about the intermolecular interactions and, particularly, the N−H···H−B dihydrogen bonding in the cases where $n =$ 1 or 2. Hence, structures are now known for all the members of the ammonia− and amine−borane series $Me_nH_{3-n}N\cdot BH_3$ ($n = 0-3$) in both the gas and solid phases. The structural variations and energetics of formation of the gaseous adducts are discussed in relation to the basicity of the $Me_nH_{3-n}N$ fragment. The relative importance of secondary interactions in the solid adducts with $n = 0-3$ has been assessed by the semi-classical density sums (SCDS-PIXEL) approach.

1. Introduction

The compound with the formal composition H_3NBH_3 has a long history[1−8] originating in the classic pioneering studies of Stock.[1] First identified as a product of the reaction between ammonia and diborane, it may be prepared, depending on the conditions, in two quite distinct forms, viz. (i) a simple molecular adduct ammonia−borane, $H_3N\cdot BH_3$, and (ii) a salt-like complex, the so-called 'diammoniate of diborane', $[(H_3N)_2BH_2]^+[BH_4]^-$. Ammonia−borane is a colorless solid that is stable at room temperature. The molecular nature of the compound is confirmed by analysis of the microwave spectrum of its vapor[9] and by X-ray[10] and neutron[11] diffraction studies of the crystalline solid. Crystallization results not only in a marked shrinkage of the B−N bond [from $r_s = 1.6576(16)$ Å[9] to $r = 1.564(6)$ Å[10]], but also in the development of short N−H···H−B intermolecular contacts (2.02 Å), affording one of the earliest examples of unconventional 'dihydrogen' bonds[12] to be recognized. This interaction between hydridic B−H and protic N−H bonds, prefiguring the potential for dihydrogen elimination, has also been signaled by Raman studies,[13] and investigated extensively through quantum chemical calculations[12,14,15] at varying levels of sophistication. These generally focus on the isolated dimer $[H_3N\cdot BH_3]_2$ or discrete oligomers[12,14] as models which do not resemble the crystal structure all that

[†] University of Oxford.
[‡] University of Edinburgh.

(1) Stock, A. *Hydrides of Boron and Silicon*; Cornell University Press: Ithaca, NY, 1933; p 58.
(2) Geanangel, R. A.; Shore, S. G. *Prep. Inorg. React.* **1966**, *3*, 123.
(3) Wiberg, E.; Amberger, E. *Hydrides of the Elements of Main Groups I-IV*; Elsevier: Amsterdam, The Netherlands, 1971.
(4) *Gmelin Handbook of Inorganic Chemistry, 8th ed., Boron Compounds, Syst. No. 13; Supplements 1−4*; Springer-Verlag: Berlin, Germany, 1974−1991.
(5) Muetterties, E. L., Ed. *Boron Hydride Chemistry*; Academic Press: New York, 1975.
(6) *Supplement to Mellor's Comprehensive Treatise on Inorganic and Theoretical Chemistry, Vol. V, Boron. Part BI: Boron-Hydrogen Compounds*; Longman: London, 1980−1981.
(7) Lane, C. F. *N-B-H Survey; Contract # DE-FC36−05GO15060; Northern Arizona University*, 2006.
(8) Stephens, F. H.; Pons, V.; Baker, R. T. *Dalton Trans.* **2007**, 2613.
(9) (a) Suenram, R. D.; Thorne, L. R. *Chem. Phys. Lett.* **1981**, *78*, 157. (b) Thorne, L. R.; Suenram, R. D.; Lovas, F. J. *J. Chem. Phys.* **1983**, *78*, 167.
(10) Bühl, M.; Steinke, T.; Schleyer, P. v. R.; Boese, R. *Angew. Chem., Int. Ed. Engl.* **1991**, *30*, 1160.
(11) Klooster, W. T.; Koetzle, T. F.; Siegbahn, P. E. M.; Richardson, T. B.; Crabtree, R. H. *J. Am. Chem. Soc.* **1999**, *121*, 6337.
(12) (a) Crabtree, R. H.; Siegbahn, P. E. M.; Eisenstein, O.; Rheingold, A. L.; Koetzle, T. F. *Acc. Chem. Res.* **1996**, *29*, 348. (b) Bakhmutov, V. I. *Dihydrogen Bonds: Principles, Experiments, and Applications*; Wiley: Hoboken, NJ, 2008.
(13) See, for example: (a) Trudel, S.; Gilson, D. F. R. *Inorg. Chem.* **2003**, *42*, 2814. (b) Custelcean, R.; Dreger, Z. A. *J. Phys. Chem. B* **2003**, *107*, 9231.
(14) See, for example: (a) Richardson, T. B.; de Gala, S.; Crabtree, R. H. *J. Am. Chem. Soc.* **1995**, *117*, 12875. (b) Cramer, C. J.; Gladfelter, W. L. *Inorg. Chem.* **1997**, *36*, 5358. (c) Popelier, P. L. A. *J. Phys. Chem. A* **1998**, *102*, 1873. (d) Kulkarni, S. A. *J. Phys. Chem. A* **1998**, *102*, 7704. (e) Li, J.; Zhao, F.; Jing, F. *J. Chem. Phys.* **2002**, *116*, 25. (f) Merino, G.; Bakhmutov, V. I.; Vela, A. *J. Phys. Chem. A* **2002**, *106*, 8491. (g) Meng, Y.; Zhou, Z.; Duan, C.; Wang, B.; Zhong, Q. *J. Mol. Struct.: THEOCHEM* **2005**, *713*, 135. (h) Nguyen, V. S.; Matus, M. H.; Grant, D. J.; Nguyen, M. T.; Dixon, D. A. *J. Phys. Chem. A* **2007**, *111*, 8844. (i) Alkorta, I.; Elguero, J.; Grabowski, S. J. *J. Phys. Chem. A* **2008**, *112*, 2721.
(15) Morrison, C. A.; Siddick, M. M. *Angew. Chem., Int. Ed.* **2004**, *43*, 4780.

closely. Only Morrison and Siddick[15] and, more recently, Miranda and Ceder[16] have tackled the problem by using a periodic quantum mechanical approach that starts with the full crystallographic unit cell as the model for calculation.

Replacing the hydrogen atoms of the ammonia fragment by methyl substituents gives in the methylamine−boranes $Me_nH_{3-n}N\cdot BH_3$ a series of molecular adducts. Every member for $n = 1-3$ resembles ammonia−borane in being a colorless solid at room temperature and has been well characterized, mainly in research carried out in the period 1935−1965;[2,3,6−8] only in the case of methylamine−borane has a salt-like form $[(MeH_2N)_2BH_2]^+[BH_4]^-$ also been described.[17] The only structure to be reported to date, however, is that of gaseous trimethylamine−borane, $Me_3N\cdot BH_3$, as determined from its gas-phase electron diffraction pattern[18] and microwave spectrum;[19] this features a B−N coordinate link measuring 1.656(2) Å (r_g),[18] very similar to that in gaseous $H_3N\cdot BH_3$. Experimental estimates of the dissociation energies, D_e, for eq 1 reveal a steady increase

$$Me_nH_{3-n}N\cdot BH_3(g) \rightarrow Me_nH_{3-n}N(g) + BH_3(g) \qquad (1)$$

with successive replacement of N−H by N−Me bonds (130, 146, 152, and 160 kJ mol^{-1} for $n = 0$, 1, 2, and 3, respectively).[20] This pattern parallels the proton affinity of the base,[21] and the values are more or less well reproduced by theoretical calculations.[22] Although no crystal structures have been reported hitherto for the methylamine−boranes $Me_nH_{3-n}N\cdot BH_3$ ($n = 1-3$), vapor pressure measurements have been made over a range of temperatures;[2,3,23] intriguingly, the enthalpies of vaporization they yield are significantly higher for $MeH_2N\cdot BH_3$ and $Me_2HN\cdot BH_3$ (79 and 77 kJ mol^{-1}) than for $Me_3N\cdot BH_3$ (57 kJ mol^{-1}), a pattern that runs counter to the polarizabilities of the molecules, if not to their dipole moments which appear to decrease with successive replacement of N−H by N−Me bonds.[3,9,19,24]

The coexistence of both hydridic B−H and protic N−H bonds in ammonia−borane and the methylamine−boranes $MeH_2N\cdot BH_3$ and $Me_2HN\cdot BH_3$, allied to a relatively strong B−N coordinate link, causes dihydrogen loss, as in eq 2, to be

$$Me_nH_{3-n}N\cdot BH_3 \rightarrow 1/m[MeNBH]_m + (3-n)H_2 \qquad (2)$$

favored over dissociation in accordance with eq 1 under most conditions. When heated or subjected to acid hydrolysis, these compounds do indeed release dihydrogen gas, but at a rate and with coproducts that depend markedly on the precise conditions. Nevertheless, the combination of low molecular weight and high gravimetric hydrogen capacity (19.6, 11.2, and 6.8 wt % for $H_3N\cdot BH_3$, $MeH_2N\cdot BH_3$, and $Me_2HN\cdot BH_3$, respectively) has attracted intense interest in them as vehicles for chemical hydrogen storage.[7,8,25,26]

In the interests of having the fullest knowledge of the compounds so as better to understand their chemistry, we have determined the crystal structure of each of the three methylamine−boranes $Me_nH_{3-n}N\cdot BH_3$ ($n = 1-3$). In addition, we have determined the structures of the gaseous molecules $MeH_2N\cdot BH_3$ and $Me_2HN\cdot BH_3$ by gas-phase electron diffraction (GED) measurements and quantum chemical calculations. Hence, the effects of methyl substitution have been investigated with regard to the structures and energetics of dissociation in molecules of the kind $Me_nH_{3-n}N\cdot BH_3$. The Edinburgh GED group, in particular, has previously been associated with research aimed at correlating the solid and vapor properties of compounds such as $[^tBuGaS]_4$.[27] Particular interest attaches not only to the structural changes that occur in the molecules on crystallization, but also, and more importantly, to the influence of intermolecular forces on the properties of the solid. To this end, the newly developed semi-classical density sums (SCDS-PIXEL) approach, which considers molecules rather than individual atoms,[28] has been applied to the crystal structures of all four compounds in the series $Me_nH_{3-n}N\cdot BH_3$ for $n = 0-3$.

2. Experimental and Computational Section

2.1. Preparation of Samples. The compounds $[MeNH_3]Cl$, $[Me_2NH_2]Cl$, $[Me_3NH]Cl$, and $LiBH_4$ (all from Aldrich, stated purities 99+%, 99%, 98%, and 95%, respectively) were purified by recrystallization, the hydrochlorides from anhydrous ethanol, and the tetrahydroborate from dry Et_2O. The adducts $MeH_2N\cdot BH_3$ (**1**), $Me_2HN\cdot BH_3$ (**2**), and $Me_3N\cdot BH_3$ (**3**) were all prepared by essentially the same method involving the reaction of the relevant hydrochloride with $LiBH_4$, both freshly recrystallized, in dry Et_2O. The procedure was generally similar to that described elsewhere for the preparation of **3**[29] and $Me_3N\cdot GaH_3$.[30] It involved adding the hydrochloride powder gradually to a stirred ethereal solution containing an equimolar quantity of $LiBH_4$ at −78 °C over a period of ca. 30 min. Stirring of the reaction mixture continued for a further 30 min before the mixture was allowed to warm up to room temperature. Under these conditions, stirring was maintained for a further 5 h in order to ensure completion of the reaction. Thereafter,

(16) Miranda, C. R.; Ceder, G. *J. Chem. Phys.* **2007**, *126*, 184703.
(17) Beachley, O. T. *Inorg. Chem.* **1965**, *4*, 1823.
(18) (a) Bauer, S. H. *J. Am. Chem. Soc.* **1937**, *59*, 1823. (b) Iijima, K.; Adachi, N.; Shibata, S. *Bull. Chem. Soc. Jpn.* **1984**, *57*, 3269.
(19) Cassoux, P.; Kuczkowski, R. L.; Bryan, P. S.; Taylor, R. C. *Inorg. Chem.* **1975**, *14*, 126.
(20) See, for example: (a) Haaland, A. *Angew. Chem., Int. Ed. Engl.* **1989**, *28*, 992, and references cited therein. (b) Lias, S. G.; Bartmess, J. E.; Liebman, J. F.; Holmess, J. L.; Levin, R. D.; Mallard, W. G. *J. Phys. Chem. Ref. Data* **1988**, *17*, Suppl. 1.
(21) Smith, B. J.; Radom, L. *J. Phys. Chem.* **1995**, *99*, 6468.
(22) See, for example: Anane, H.; Jarid, A.; Boutalib, A.; Nebot-Gil, I.; Tomás, F *J. Mol. Struct.: THEOCHEM* **1998**, *455*, 51.
(23) (a) Schlesinger, H. I.; Ritter, D. M.; Burg, A. B. *J. Am. Chem. Soc.* **1938**, *60*, 1296. (b) Alton, E. R.; Brown, R. D.; Carter, J. C.; Taylor, R. C. *J. Am. Chem. Soc.* **1959**, *81*, 3550. (c) Chickos, J. S.; Acree, W. E., Jr. *J. Phys. Chem. Ref. Data* **2002**, *31*, 634–5.
(24) Nöth, H.; Beyer, H. *Chem. Ber.* **1960**, *93*, 939.
(25) See, for example: (a) Fakioğlu, E.; Yürüm, Y.; Nejat Veziroğlu, T. *Int. J. Hydrogen Energy* **2004**, *29*, 1371. (b) Gutowska, A.; Li, L.; Shin, Y.; Wang, C. M.; Li, X. S.; Linehan, J. C.; Smith, R. S.; Kay, B. D.; Schmid, B.; Shaw, W.; Gutowski, M.; Autrey, T. *Angew. Chem., Int. Ed.* **2005**, *44*, 3578. (c) Bluhm, M. E.; Bradley, M. G.; Butterick, R., III; Kusari, U.; Sneddon, L. G. *J. Am. Chem. Soc.* **2006**, *128*, 7748. (d) Baitalow, F.; Wolf, G.; Grolier, J.-P. E.; Dan, F.; Randzio, S. L. *Thermochem. Acta* **2006**, *445*, 121. (e) Cheng, F.; Ma, H.; Li, Y.; Chen, J. *Inorg. Chem.* **2007**, *46*, 788. (f) Keaton, R. J.; Blacquiere, J. M.; Baker, R. T. *J. Am. Chem. Soc.* **2007**, *129*, 1844. (g) Stephens, F. H.; Baker, R. T.; Matus, M. H.; Grant, D. J.; Dixon, D. A. *Angew. Chem., Int. Ed.* **2007**, *46*, 746. (h) Stowe, A. C.; Shaw, W. J.; Linehan, J. C.; Schmid, B.; Autrey, T. *Phys. Chem. Chem. Phys.* **2007**, *9*, 1831. (i) Mohajeri, N.; T-Raissi, A.; Adebiyi, O. *J. Power Sources* **2007**, *167*, 482. (j) Nguyen, M. T.; Nguyen, V. S.; Matus, M. H.; Gopakumar, G.; Dixon, D. A. *J. Phys. Chem. A* **2007**, *111*, 679. (k) Marder, T. B. *Angew. Chem., Int. Ed.* **2007**, *46*, 8116. (l) Yan, J.-M.; Zhang, X.-B.; Han, S.; Shioyama, H.; Xu, Q. *Angew. Chem., Int. Ed.* **2008**, *47*, 2287.
(26) Dixon, D. A.; Gutowski, M. *J. Phys. Chem. A* **2005**, *109*, 5129.
(27) (a) Cleaver, W. M.; Späth, M.; Hnyk, D.; McMurdo, G.; Power, M. B.; Stuke, M.; Rankin, D. W. H.; Barron, A. R. *Organometallics* **1995**, *14*, 690. (b) Power, M. B.; Barron, A. R.; Hnyk, D.; Robertson, H. E.; Rankin, D. W. H. *Adv. Mater. Opt. Electron.* **1995**, *5*, 177.
(28) (a) Dunitz, J. D.; Gavezzotti, A. *Angew. Chem., Int. Ed.* **2005**, *44*, 1766. (b) Gavezzotti, A. *Molecular Aggregation: Structure Analysis and Molecular Simulation of Crystals and Liquids*; Oxford University Press: Oxford; New York, 2007. (c) Gavezzotti, A. *Z. Kristallogr.* **2005**, *220*, 499. (d) Gavezzotti, A. *J. Chem. Theory Comput.* **2005**, *1*, 834. (e) Wood, P. A.; Francis, D.; Marshall, W. G.; Moggach, S. A.; Parsons, S.; Pidcock, E.; Rohl, A. *CrystEngComm.* **2008**, *10*, 1154.
(29) Schaeffer, G. W.; Anderson, E. R. *J. Am. Chem. Soc.* **1949**, *71*, 2143.
(30) Shriver, D. F.; Shirk, A. E. *Inorg. Synth.* **1977**, *17*, 42.

Table 1. Crystallographic Data for Compounds **1**, **2**, and **3**

param	1	2	3
empirical formula	CH_8BN	$C_2H_{10}BN$	$C_3H_{12}BN$
fw	44.89	58.92	72.95
cryst dimens (mm)	0.40 × 0.20 × 0.04	0.50 × 0.20 × 0.05	0.50 × 0.30 × 0.20
cryst syst	orthorhombic	monoclinic	rhombohedral
space group	*Pnma*	$P2_1/c$	$R3m$
unit cell dimens			
a (Å)	11.1350(8)	7.0452(6)	9.0792(5)
b (Å)	6.5575(4)	5.8368(5)	9.0792(5)
c (Å)	4.9194(3)	12.2335(14)	5.8922(5)
α (deg)	90	90	90
β (deg)	90	104.648(4)	90
γ (deg)	90	90	120
V (Å^3)	359.20(4)	486.71(8)	420.63(5)
Z	4	4	3
d_{calcd} (Mg m^{-3})	0.830	0.804	0.864
abs coeff (mm^{-1})	0.048	0.046	0.049
θ_{max} (deg)	31.987	27.504	27.463
reflns measd	1813	2185	599
unique reflns (R_{int})	663 (0.037)	1104 (0.034)	130 (0.024)
no. of params	38	77	24
conventional R [$R > 4\sigma(F)$]	0.0381	0.0416	0.0283
weighted R (F^2 and all data)	0.1054	0.1120	0.0738
GOF on F^2 (S)	1.0019	1.0032	1.0092
largest diff. peak/hole (e Å^{-3})	+0.23/−0.11	+0.11/−0.11	+0.10/−0.10

the mixture was cooled to −45 °C and the ether removed under vacuum. The white powder remaining was heated in vacuo to temperatures ranging from 80 °C, through 65 °C, to 50 °C to give a sublimate of **1**, **2**, and **3**, respectively. The purity of each product was checked by reference to its Raman spectrum and to the ^{1}H and ^{11}B NMR spectra of a tetrahydrofuran-d_8 solution.[2−4] Yields ranged from 70% for **1** to 78% for **3** in relation to the quantities of the reagents taken and reaction 3.

$$LiBH_4 + [Me_nNH_{4-n}]Cl \rightarrow Me_nH_{3-n}N \cdot BH_3 + LiCl + H_2 \quad (3)$$

2.2. Gas-Phase Electron Diffraction. Electron scattering intensities were measured for the vapors of **1** and **2** using the Edinburgh GED apparatus.[31] An accelerating voltage of 40 kV was used, resulting in an electron wavelength of ∼0.06 Å. The intensities were recorded on Kodak Electron Image films at two nozzle-to-film distances to maximize the scattering angle over which data were collected. Although there exists a port that allows data to be collected at a shorter nozzle-to-film distance, suitable vapor pressures were not attainable below the decomposition temperature. In order to obtain suitable vapor pressures and to prevent condensation in the nozzle, the sample and nozzle were heated to the temperatures listed in Table S1.

The photographic films were scanned using an Epson Expression 1680 Pro flatbed scanner as part of a method that is now used routinely in Edinburgh and described elsewhere.[32] Data-reduction and least-squares refinement processes were carried out using the ed@ed program[33] employing the scattering factors of Ross et al.[34] The weighting points for the off-diagonal weight matrices, correlation parameters, and scale factors are given in Table S1.

2.3. X-ray Diffraction. Crystals of **1**, **2**, and **3** were each grown from an Et_2O solution kept at 0−4 °C over a period of days. Single crystals were each mounted under perfluoropolyether oil on a glass fiber and cooled rapidly to 150 K. X-Ray diffraction data [λ(Mo Kα) = 0.710 73 Å] were then collected on an Enraf-Nonius Kappa CCD diffractometer. Table 1 gives the crystal data and other information relating to the structure determination and refinement for **1**−**3**. Crystal structures were solved by direct methods using SIR92[35] and refined using CRYSTALS.[36] Hydrogen atoms were located in difference maps and refined subject to restraints. Structures were visualized using DIAMOND[37] and MERCURY,[38] and miscellaneous geometry calculations were carried out using PLATON.[39]

2.4. Computational Methods. 2.4.1. Properties of the Isolated Molecules. All calculations were performed using the resources of the NSCCS[40] and the EaStCHEM Research Computing Facility[41] running the Gaussian 03 suite of programs.[42] For each of the molecules of **1** and **2**, a single minimum was identified on the potential-energy surface representing a C_s-symmetric structure. With the symmetry fixed, geometries were optimized, first at the spin-restricted Hartree−Fock level of theory with the 3-21G* basis set[43] on all atoms followed by the 6-31G* basis set[44] and then

(31) Huntley, C. M.; Laurenson, G. S.; Rankin, D. W. H. *J. Chem. Soc., Dalton Trans.* **1980**, 954.
(32) Fleischer, H.; Wann, D. A.; Hinchley, S. L.; Borisenko, K. B.; Lewis, J. R.; Mawhorter, R. J.; Robertson, H. E.; Rankin, D. W. H. *Dalton Trans.* **2005**, 3221.
(33) Hinchley, S. L.; Robertson, H. E.; Borisenko, K. B.; Turner, A. R.; Johnston, B. F.; Rankin, D. W. H.; Ahmadian, M.; Jones, J. N.; Cowley, A. H. *Dalton Trans.* **2004**, 2469.
(34) Ross, A. W.; Fink, M.; Hilderbrandt, R. In *International Tables for Crystallography*; Wilson, A. J. C., Ed.; Kluwer Academic Publishers: Dordrecht, The Netherlands, 1992: Vol. 2, p 245.
(35) SIR 92: Altomare, A; Cascarano, G.; Giacovazzo, C.; Guagliardi, A. J. *J. Appl. Crystallogr.* **1993**, *26*, 343.
(36) CRYSTALS: Betteridge, P. W.; Carruthers, J. R.; Cooper, R. I.; Prout, K.; Watkin, D. J. *J. Appl. Crystallogr.* **2003**, *36*, 1487.
(37) DIAMOND: Brandenburg, K.; Putz, H. *DIAMOND*; Crystal Impact: Bonn, Germany, 2005.
(38) MERCURY: Macrae, C. F.; Bruno, I. J.; Chisholm, J. A.; Edgington, P. R.; McCabe, P.; Pidcock, E.; Rodriguez-Monge, L.; Taylor, R.; van de Streek, J.; Wood, P. A. *J. Appl. Crystallogr.* **2008**, *41*, 466.
(39) PLATON: Spek, A. L. *J. Appl. Crystallogr.* **2003**, *36*, 7.
(40) National Service for Computational Chemistry Software (NSCCS). URL http://www.nsccs.ac.uk.
(41) EaStCHEM Research Computing Facility (http://www.eastchem.ac.uk/rcf). This facility is partially supported by the eDIKT initiative (http://www.edikt.org).
(42) Frisch, M. J. et al. *Gaussian 03, Revision C.02*; Gaussian, Inc.: Wallingford, CT, 2004.
(43) (a) Binkley, J. S.; Pople, J. A.; Hehre, W. J. *J. Am. Chem. Soc.* **1980**, *102*, 939. (b) Gordon, M. S.; Binkley, J. S.; Pople, J. A.; Pietro, W. J.; Hehre, W. J. *J. Am. Chem. Soc.* **1982**, *104*, 2797. (c) Pietro, W. J.; Francl, M. M.; Hehre, W. J.; DeFrees, D. J.; Pople, J. A.; Binkley, J. S. *J. Am. Chem. Soc.* **1982**, *104*, 5039.
(44) (a) Hehre, W. J.; Ditchfield, R.; Pople, J. A. *J. Chem. Phys.* **1972**, *56*, 2257. (b) Hariharan, P. C.; Pople, J. A. *Theor. Chim. Acta* **1973**, *28*, 213. (c) Gordon, M. S. *Chem. Phys. Lett.* **1980**, *76*, 163.

Table 2. Selected Calculated Parameters for $Me_nH_{3-n}N\cdot BH_3$ ($n = 0-3$)[a]

	B−N			<N−B−H	ΣB	ΣN
	MP2(full)/ 6-311++G**	MP2(full)/ aug-cc-pVTZ	MP2(full)/ aug-cc-pVQZ	MP2(full)/ 6-311++G**	MP2(full)/ 6-311++G**	MP2(full)/ 6-311++G**
Me_3NBH_3	1.638	−	1.624[b]	105.2	339.9	327.6
Me_2HNBH_3	1.633	1.623	1.619	104.8/105.3	340.2	326.8
MeH_2NBH_3	1.639	1.628	1.624	104.9/105.2	340.7	325.7
H_3NBH_3	1.653	1.645	1.639	104.8	341.1	323.4

[a] Distances are in Å; angles are in deg. [b] This value has been estimated on the basis that the MP2(full)/aug-cc-pVQZ value is consistently shorter than the MP2(full)/6-311++G** value by 0.014(1) Å.

using MP2[45] to include the energy due to electron correlation. At this level the 6-311G* and 6-311++G** basis sets[46] were also used, as were aug-cc-pVnZ ($n = D, T, Q$) basis sets.[47] All-electron MP2 calculations [MP2(full)] were used throughout this work. Force constants calculated at the RHF/6-31G* level were subsequently employed, along with the program SHRINK,[48] to obtain initial amplitudes of vibration, and third derivatives of the energy (giving cubic anharmonicity terms)[49] were then employed to give curvilinear perpendicular distance correction terms for the GED refinement. Thus, the structures obtained from the refinements are of the type $r_{a3,1}$. For a full discussion of the a3,1 nomenclature see ref 50. For the purposes of estimating r_{h1} values from existing experimental data, harmonic force fields were calculated at the MP2(full)/aug-cc-pVDZ level.

2.4.2. Properties of the Crystalline Solids. Lattice and intermolecular interaction energies were evaluated for compounds in the series $Me_nH_{3-n}N\cdot BH_3$, with $n = 0-3$, by means of the semiclassical density sums (SCDS-PIXEL) method.[28,51] The geometry of each molecule was taken from the relevant crystal structure, the N−H and B−H distances we have determined by X-ray diffraction being extended to standard neutron lengths.[52] Without optimizing the geometry, an electron density map was then calculated on a three-dimensional grid with a step size of 0.08 Å for the molecule at the MP2/6-31G** level using Gaussian 03.[42] The resulting density map was produced on a three-dimensional grid with a step size of 0.08 Å. The pixels were then 'condensed' into superpixels with dimensions 0.24 × 0.24 × 0.24 Å to expedite subsequent calculations (this is referred to as 'condensation level 3').[28b,51] The next stage of the calculations was to generate a cluster of molecules about a central reference molecule extending to 14 Å, as the basis for the intermolecular energy calculations. In order to determine the accuracy of the PIXEL procedure for boron compounds, calculations were also carried out on the following compounds for which both crystal structures and experimental sublimation energies are available (the CSD refcodes for the structural data are given in brackets):[53] B_2F_4 (unpublished crystal structure data), Me_2NBF_2 (DMABDF), pyridine−BBr_3 (BUNGEW), BPh_3 (TPHBOR), $B_3N_3H_3Cl_3$ (FUYTEY), and $B_3H_{12}N_3$ (FUZPAR). Sublimation energies were taken from the compilation by Chickos and Acree.[23c]

How these calculations proceeded can be illustrated using the Coulombic energy term. Intermolecular Coulombic energies in the cluster were calculated as sums of pixel−pixel, pixel−nucleus, and nucleus−nucleus terms, each pixel and each atomic nucleus having its own charge. Each interaction was evaluated on the basis of the standard electrostatic potential energy expression for two charges q_1 and q_2 separated by a distance r, i.e., eq 4:

$$E_{\mathrm{Coul}} = \frac{q_1 q_2}{4\pi\varepsilon_0 r} \tag{4}$$

Pixel-by-pixel summations of the polarization, dispersion, and repulsion energies were calculated via an analogous procedure, although this required the introduction of a total of four empirical parameters that had been previously optimized to reproduce experimental sublimation enthalpies for a range of organic molecular crystals.[28b] It should be explained here that the repulsion term corresponds to what is often referred to as 'Born' repulsion, that is, a quantum mechanical effect arising from overlap of charge clouds; ordinary electrostatic repulsion is part of the Coulombic term. Tests have shown that PIXEL results for organic systems compare well with the results of intermolecular perturbation theory and DFT calculations.[28b,e]

The PIXEL calculations yielded a total lattice energy derived from the sum of four components, namely, the electrostatic or Coulombic, polarization, dispersion, and repulsion terms, a correction being needed for structures in polar space groups.[54] Individual intermolecular contact energies were also calculated; in common with all the other energies, these are broken down into the four components already listed. This dissection into physically meaningful component terms is particularly valuable in any analysis of intermolecular interactions in the crystalline phase. However, it is important to recognize that PIXEL treats interactions at a *molecular* and not at an atomic level, and one must beware of falling into the trap of attributing a particular contact energy to a single prominent interatomic interaction, such as a hydrogen bond.

Calculation of Hirshfeld surfaces and associated electrostatic potentials was accomplished using CrystalExplorer.[55]

3. Results and Discussion

3.1. Isolated Molecules: Calculations and GED Results. 3.1.1. Calculations. The geometries of the molecules $Me_nH_{3-n}N\cdot BH_3$ ($n = 0-3$) were calculated using a variety of basis sets. As shown in Table 2, the B−N distances in the methylamine−boranes are very similar, while that in $H_3N\cdot BH_3$ is slightly longer. The most notable finding, however, was the basis-set dependence of the B−N distances. At the same level of theory, the use of augmented correlation-consistent quadruple-ζ basis sets shortens these bonds by around 0.015 Å compared with the use of a large Pople-style basis set. In all

(45) Møller, C.; Plesset, M. S. *Phys. Rev.* **1934**, *46*, 618.
(46) (a) Krishnan, R.; Binkley, J. S.; Seeger, R.; Pople, J. A. *J. Chem. Phys.* **1980**, *72*, 650. (b) McLean, A. D.; Chandler, G. S. *J. Chem. Phys.* **1980**, *72*, 5639.
(47) (a) Dunning, T. H., Jr. *J. Chem. Phys.* **1989**, *90*, 1007. (b) Kendall, R. A.; Dunning, T. H., Jr.; Harrison, R. J. *J. Chem. Phys.* **1992**, *96*, 6796.
(48) (a) Sipachev, V. A. *J. Mol. Struct. (THEOCHEM)* **1985**, *121*, 143. (b) Sipachev, V. A. *J. Mol. Struct.* **2001**, *567*, 67.
(49) (a) Barone, V. *J. Chem. Phys.* **2005**, *122*, 014108. (b) Barone, V. *J. Chem. Phys.* **2004**, *120*, 3059.
(50) McCaffrey, P. D.; Mawhorter, R. J.; Turner, A. R.; Brain, P. T.; Rankin, D. W. H. *J. Phys. Chem. A* **2007**, *111*, 6103.
(51) Gavezzotti, A. *OPiX: a computer program package for the calculation of intermolecular interactions and crystal energies*; University of Milan: Milan, Italy, 2003.
(52) Desiraju, G.; Steiner, T. *The Weak Hydrogen Bond in Structural Chemistry and Biology*; Oxford University Press: Oxford; New York, 2001.
(53) Allen, F. H. *Acta Crystallogr., Sect. B: Struct. Sci.* **2002**, *B58*, 380.
(54) van Eijck, B. P.; Kroon, J. *J. Phys. Chem. B* **1997**, *101*, 1096.
(55) Wolff, S. K.; Grimwood, D. J.; McKinnon, J. J.; Jayatilaka, D.; Spackman, M. A. *Crystal_Explorer, version 2.1(381)*; University of Western Australia: Perth, Australia, 2007.

Table 3. Refined ($r_{a3,1}$) and Calculated (r_e) Geometric Parameters for **1** and Its Dissociation Products $MeNH_2$ and B_2H_6 the GED Study[a,b]

	param	$r_{a3,1}$	r_e	restraint
Independent				
p_1	rC−H mean	1.112(7)	1.083	0.01
p_2	rN−H	1.025(10)	1.012	0.01
p_3	rB−H mean	1.208(10)	1.205	0.01
p_4	rC−N	1.449(3)	1.468	−
p_5	rN−B	1.602(7)	1.624	−
p_6	∠H−N−H	106.4(11)	106.4	1.0
p_7	∠N−C−H average	109.5(7)	109.9	1.0
p_8	∠N−C−H difference	3.9(6)	3.8	0.5
p_9	∠H−C−H	110.0(11)	110.2	1.0
p_{10}	∠N−B−H average	103.9(9)	105.3	1.0
p_{11}	∠H−B−H difference	0.5(5)	0.5	0.5
p_{12}	∠H−B−H	113.5(11)	113.5	1.0
p_{13}	∠X−N−C[c]	125.9(8)	124.8	1.0
p_{14}	∠X−N−B[c]	122.7(8)	121.8	1.0
p_{15}	∠B−H−B bridging	94.0(9)	95.6	1.0
p_{16}	rB−H bridging	1.329(10)	1.316	0.01
p_{17}	rB−H terminal	1.188(11)	1.180	0.01
p_{18}	∠H−B−H terminal	122.4(11)	122.4	1.0
p_{19}	proportion of molecules intact	0.67[d]	−	−
Dependent				
p_{20}	∠N−C−H(9)	111.4(7)	111.8	−
p_{21}	∠N−C−H(10)	107.6(7)	108.0	−
p_{22}	∠N−B−H(5)	103.6(10)	105.0	−
p_{23}	∠N−B−H(6)	104.2(9)	105.5	−
p_{24}	∠B−N−C	111.4(5)	113.4	−

[a] Refers to an MP2(full)/aug-cc-pVQZ calculation. [b] Distances (r) are in Å, angles (∠) in deg. See text for parameter definitions and Figure 1a for atom numbering. The figures in parentheses are the estimated standard deviations of the last digits. [c] X is a dummy atom lying halfway between H(2) and H(3). [d] See text for description of this parameter.

cases, the staggered conformation is the only minimum. At this point we must acknowledge the superior computational work of Dixon and Gutowski,[26] who have calculated the B−N distance in $H_3N \cdot BH_3$ using CCSD(T)/aug-cc-VTZ. Their value of 1.6575 Å differs by 0.01 Å from that we obtain at the MP2(full) level of theory.

3.1.2. GED Studies: Structures of the Gaseous Molecules 1 and 2. Determining the structure of gaseous **1** was initially hampered by its propensity to dissociate partially at the temperatures required to obtain a suitably high vapor pressure. This is described in more detail in the Supporting Information.

The model that was used in the refinement described the structures of **1** and the dissociation products MeH_2N and B_2H_6. To simplify matters, and guided by the results from high-level ab initio calculations, the parameters describing the amino group in **1** were also used to describe MeH_2N, with but one modification described in the Supporting Information. Both **1** and MeH_2N were modeled with C_s symmetry and B_2H_6 with D_{2h} symmetry. The set of parameters used in the model is listed in Table 3; the atom numbering used to define **1** is shown in Figure 1a. A full description of the model used is given in the Supporting Information.

On the basis of the calculations described above, a C_s-symmetric model was written to describe the geometry of **2**. The atom numbering used in the descriptions of the parameters is shown in Figure 1b, and the parameters are listed in Table 4. Again, a full description of the model is given in the Supporting Information.

For both **1** and **2**, all the independent geometric parameters were refined using a least-squares method, and restraints were

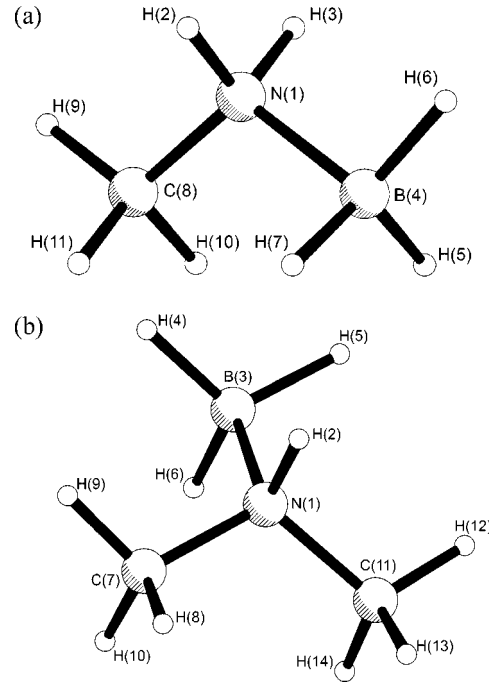

Figure 1. Molecular structure, including numbering scheme used in the GED studies (a) of **1** and (b) of **2**.

Table 4. Refined ($r_{a3,1}$) and Calculated (r_e) Geometric Parameters for **2** from the GED Study[a,b]

	param	$r_{a3,1}$	r_e	restraint
Independent				
p_1	rC−H mean	1.080(2)	1.084	−
p_2	rN−H	1.023(9)	1.014	0.01
p_3	rB−H mean	1.216(7)	1.206	0.01
p_4	rC−N	1.467(2)	1.467	−
p_5	rN−B	1.615(4)	1.619	−
p_6	∠B−N−C	111.9(2)	111.5	−
p_7	∠N−C−H average	110.6(3)	109.1	−
p_8	∠N−C−H difference 1	2.7(5)	2.8	0.5
p_9	∠N−C−H difference 2	1.0(5)	1.2	0.5
p_{10}	∠H−C−H average	109.8(9)	109.6	1.0
p_{11}	∠H−C−H difference	1.4(5)	1.4	0.5
p_{12}	∠N−B−H average	105.8(9)	105.2	−
p_{13}	∠N−B−H difference	0.7(5)	0.9	0.5
p_{14}	∠H−B−H	113.5(10)	113.4	1.0
p_{15}	∠H−N−C	107.2(5)	108.2	1.0
p_{16}	∠H−N−B	105.8(9)	106.1	1.0
Dependent				
p_{17}	∠C−N−C	112.4(4)	111.0	−
p_{18}	∠N−C(7)-H(8)	112.2(4)	111.0	−
p_{19}	∠N−C(7)-H(9)	110.2(4)	108.8	−
p_{20}	∠N−C(7)-H(10)	109.2(4)	107.6	−
p_{21}	∠H(8)−C(7)−H(10)	110.5(10)	110.5	−
p_{22}	∠H(9)−C(7)−H(10)	109.1(10)	108.9	−
p_{23}	∠N−B−H(4)	106.2(9)	105.6	−
p_{24}	∠N−B−H(6)	105.5(10)	104.7	−

[a] Refers to an MP2(full)/aug-cc-pVQZ calculation. [b] Distances (r) are in Å, angles (∠) in deg. See text for parameter definitions and Figure 1b for atom numbering. The figures in parentheses are the estimated standard deviations of the last digits.

applied, using the SARACEN method,[56] to parameters (mainly those involving hydrogen, which is often poorly defined) that could not otherwise be refined (Tables 3 and 4). The restraints were based on values calculated at the MP2(full)/aug-cc-pVQZ level, and the uncertainties were loosely derived with reference to the change in value of that parameter during the series of calculations performed. Additionally, groups of amplitudes of

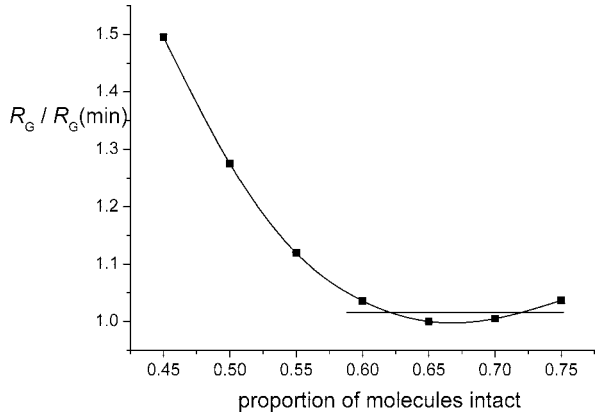

Figure 2. Plot of R_G/R_G(min) versus proportion of molecules of **1** that do not undergo dissociation. The horizontal line marks the 95% confidence limit.

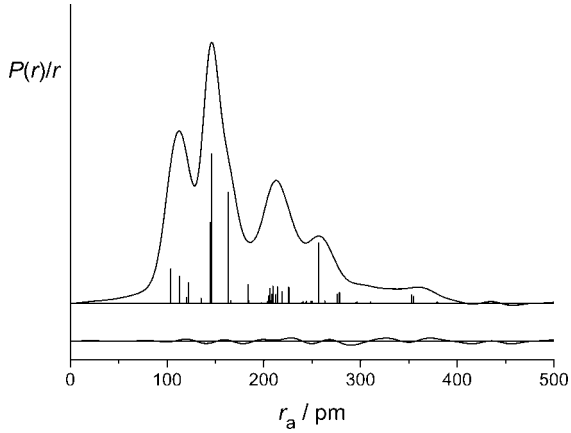

Figure 3. Experimental radial-distribution curves and theoretical-minus-experimental difference curves for **1** and its dissociation products. Before Fourier inversion, the data were multiplied by $s\cdot\exp(-0.00002s^2)/(Z_C - f_C)(Z_N - f_N)$.

vibration were refined (see Tables S2 and S3 for lists of amplitudes of vibration for **1** and **2**, respectively).

In the case of **1**, a parameter was included to describe the proportion of the molecules that do not undergo dissociation. It was found that the lowest *R* factor was obtained for a proportion of 0.67. To estimate the uncertainty on this value, the *R* factor was recorded at a number of values either side of 0.67, R_G/R_G(min) was plotted against the proportion of **1** (Figure 2), and, with reference to Hamilton's tables,[57] a line was drawn at 1.016 representing the 95% confidence limit. This suggests that the fraction of molecules of **1** remaining intact under the conditions of the experiment was $\sim 0.67 \pm 0.03$. The study of **1** and its dissociation products gave GED data that were rather noisy, and the fairly crude attempt to fit three separate species to the data has resulted in larger-than-usual *R* factors ($R_G = 0.110$, $R_D = 0.061$). For this refinement, the radial-distribution curves are given in Figure 3, the molecular-scattering intensity curves in Figure S1.

No such problems of dissociation were experienced with the dimethylamine adduct **2**. The success of the refinement of the

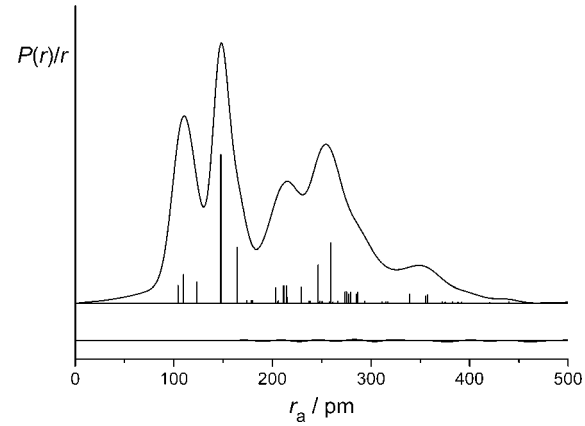

Figure 4. Experimental radial-distribution curves and theoretical-minus-experimental difference curves for **2**. Before Fourier inversion, the data were multiplied by $s\cdot\exp(-0.00002s^2)/(Z_C - f_C)(Z_N - f_N)$.

Table 5. Comparison of Differently Defined B−N Distances for $Me_nH_{3-n}N\cdot BH_3$ ($n = 1-3$)[a]

adduct	r_a	r_g	r_{h1}	$r_{a3,1}$
$MeH_2N\cdot BH_3$	1.634(7)	1.637(7)	1.633(7)	1.602(7)
$Me_2HN\cdot BH_3$	1.644(4)	1.646(4)	1.642(4)	1.615(4)
$Me_3N\cdot BH_3$	1.653(2)	1.656(2)	1.652(2)	1.623(2)

[a] See text for details of how distances were calculated. All distances are in Å.

relevant parameters in this case can be assessed numerically by the final *R* factor, which was $R_G = 0.027$ ($R_D = 0.021$), and visually by the goodness of fit of the radial-distribution and difference curves as displayed in Figure 4, and the molecular-scattering intensity curves (Figure S2).

The least-squares correlation matrices for **1** and **2** are given in Tables S4 and S5, and coordinates for the final GED structures and for the calculated structure [MP2(full)/aug-cc-pVQZ] are in Tables S6 and S7 and Tables S8 and S9, respectively.

3.1.3. Comparisons of the Structures of the Isolated $Me_nH_{3-n}N\cdot BH_3$ Molecules ($n = 1-3$). Although GED[58,59] and microwave spectroscopic[60−62] studies have been carried out previously for **3**, microwave studies have been carried out for $H_3N\cdot BH_3$,[9] and considerable effort has been put into calculating the structures of all the members of the family $Me_nH_{3-n}N\cdot BH_3$ ($n = 1-3$),[22] the present studies afford the first experimental results regarding the structures of gaseous **1** and **2**. Various distances determined by the different methods are listed in Table 5. Direct comparison is complicated by the fact that different distances (r_e from computational methods; r_a, r_g, r_{h1}, and $r_{a3,1}$ from GED experiments; r_0 and r_s from microwave spectroscopic studies) have different physical meanings. This explains why, wherever possible, we have taken the literature values and estimated the chosen distances using calculated corrections.

Our work has involved geometry optimizations to determine the structures of these molecules using a variety of computational methods and basis sets, as described in the Experimental and Computational Section. Our conclusion is that some features

(56) (a) Blake, A. J.; Brain, P. T.; McNab, H.; Miller, J.; Morrison, C. A.; Parsons, S.; Rankin, D. W. H.; Robertson, H. E.; Smart, B. A. *J. Phys. Chem.* **1996**, *100*, 12280. (b) Brain, P. T.; Morrison, C. A.; Parsons, S.; Rankin, D. W. H. *J. Chem. Soc., Dalton Trans.* **1996**, 4589. (c) Mitzel, N. W.; Rankin, D. W. H. *Dalton Trans.* **2003**, 3650.
(57) Hamilton, W. C. *Acta Crystallogr.* **1965**, *18*, 502.
(58) Bauer, S. H. *J. Am. Chem. Soc.* **1937**, *59*, 1804.
(59) Iijima, K.; Adachi, N.; Shibata, S. *Bull. Chem. Soc. Jpn.* **1984**, *57*, 3269.
(60) Schirdewahn, H. G. *Ph.D. Thesis*, University of Freiburg, 1965.
(61) Durig, J. R.; Li, Y. S.; Odom, J. D. *J. Mol. Struct.* **1973**, *16*, 443.
(62) Cassoux, P.; Kuczkowski, R. L.; Bryan, P. S.; Taylor, R. C. *Inorg. Chem.* **1975**, *14*, 126.

of the structures are very dependent on the size of the basis sets used and also, but to a lesser degree, on the level of theory used. At the highest level and with the largest basis sets used [MP2(full)/aug-cc-pVQZ], many of the calculated geometric parameters for **2** are close to those determined using GED ($r_{a3,1}$). This gives us some confidence in the results of our GED experiment.

The $r_{a3,1}$ values for the B−N distances determined for **1** [1.602(7) Å] and for **2** [1.615(4) Å] appear to be rather short when compared with the experimental value for the B−N distance obtained from the combined GED and MW study of gaseous **3** ($r_g = 1.656 \pm 0.002$ Å).[59] The origin of the short $r_{a3,1}$ values for **1** and **2** can be traced, however, to the corrections of 0.033 and 0.029 Å, respectively, that have been applied to the vibrationally averaged r_a values yielded by the GED experiments (Tables S2 and S3). Such corrections have been derived from anharmonic force fields calculated at the RHF/6-31G* level, as described earlier. To investigate this further, harmonic force fields [MP2(full)/aug-cc-pVDZ] were used to generate corrections that, when applied to the r_a distance, yielded r_{h1} distances. For **1** and **2**, the corrections, k_{h1}, were 0.0035 and 0.0036 Å and, because $r_{h1} \approx r_a + u^2/r_a - k_{h1}$, the r_{h1} values for the B−N distances determined for **1** and **2** are estimated to be 1.633(7) and 1.642(4) Å, respectively. The B−N bonds are subject therefore to distinctly anharmonic vibrations, a factor not obvious from the vibrationally averaged r_a distance, or from the often-quoted r_{h1} and r_g distances. Moreover, the $r_{a3,1}$ values for **1** and **2** agree well with the results of high-level ab initio calculations [MP2(full)/aug-cc-pVQZ]. The significant anharmonicity of the B−N stretching vibration in $H_3N\cdot BH_3$ has been studied by Jagielska et al.,[63] who by performing a one-dimensional full quantum calculation of this mode obtained a frequency that differed by only 4% from the experimental value, as opposed to 32% using the harmonic approximation.

A search for previous studies of gaseous **3** reveals that the structure was first studied in 1937 by GED,[58] then once in the 1960s,[60] twice in the 1970s[61,62] using microwave spectroscopy, and again in 1984 using a combination of new GED data with the rotation constants determined in the more recent microwave study.[59] Unsurprisingly, these studies report a range of B−N distances: 1.62 ± 0.05,[58] 1.65 ± 0.02,[60] 1.609 or 1.637[61] (with the authors suggesting that the former is more believable), 1.638 ± 0.01,[62] and 1.656 ± 0.002 Å.[59] In the present discussion, we will concentrate on the most recent GED data and the microwave study that yielded the rotation constants used with these data. The distance 1.656 ± 0.002 Å is of the type r_g ($r_g \approx r_a + u^2/r_a$), and has been determined using a combination of GED data with microwave rotation constants.[59] Although the r_a value is not given, the amplitude of vibration, u, is known, and so an r_a value of 1.653 Å can be estimated. In the same way that we obtained corrections to find $r_{a3,1}$ distances for **2** and **1**, we have used an anharmonic force field (RHF/6-31G*) and SHRINK to provide a correction for **3**. On this basis, we estimate $r_{a3,1}$B−N to be 1.623(2) Å, a value satisfyingly close to that determined by high-level ab initio calculations.

On the evidence of the quantum chemical calculations, the B−N distance (r_e) in amine−borane adducts of the type $Me_nH_{3-n}N\cdot BH_3$ varies but little with progressive methylation at the nitrogen center (spanning a total range not exceeding 0.006 Å), while $H_3N\cdot BH_3$ displays a distance about 0.02 Å longer than that in any of the methylamine−boranes. Refinement of the GED data for the methylamine−boranes under the SARACEN protocol[56] yields B−N distances (r_a, r_g, r_{hl}, etc.) that become slightly longer—by about 0.02 Å—as n increases from 1 to 3 (see Table 5). It should be appreciated, however, that partial dissociation causes the estimate for **1** to be relatively poorly defined compared with those for **2** and **3**. As a test of this issue, the B−N distance in **1** was deliberately restrained to the calculated value of 1.624 Å, with a fairly tight uncertainty of ± 0.005 Å. In fact, this had little effect on the refinement, raising the R_G factor by 0.02 and giving rise to negligible changes in the other parameters. We are bound to conclude therefore that the B−N distance is not a sensitive reporter on the coordinate link in this series of molecules. With no GED data to guide us, $H_3N\cdot BH_3$ cannot easily be compared with the methylamine−boranes, but the B−N distance determined from its microwave spectrum [$r_s = 1.6576(16)$ Å][9] is consistent with the results of the present theoretical calculations in its implication that the B−N bond is indeed somewhat longer in this case. During the preparation of this manuscript, a further article on the structure of $H_3N\cdot BH_3$ appeared in the literature.[64] This paper, reporting the results of very high-level calculations using both MP2 and CCSD(T) theory, concludes that the equilibrium distance for B−N is 1.6455 Å. Furthermore, the authors use a calculated force field to obtain corrections that they then apply to the literature rotation constants for the molecule. As a result, they quote a semiempirical B−N bond length of 1.6453 Å.

The combination of experiment and theory also shows that increasing charge transfer from N to B in the series $Me_nH_{3-n}N\cdot BH_3$ manifests itself in small changes (amounting to no more than 1−3°) in the N−B−H and B−N−C/B−N−H angles. Thus, the $Me_nH_{3-n}N$ unit becomes less pyramidal as BH_3 becomes more pyramidal with increasing n, as revealed for example in Table 2 listing the calculated sums of the angles subtended by the substituents at N (ΣN) and at B (ΣB). The barriers to rotation of the BH_3 group about the B−N bond have been calculated at the MP2(full)/6-311++G** level for each of the molecules in the series $Me_nH_{3-n}N\cdot BH_3$; they are 9.9, 11.8, 14.3, and 19.1 kJ mol^{-1} as n runs from 0 to 3. Progressing from $H_3N\cdot BH_3$ through the series to **3** is attended by the following calculated energies (E_{diss}/E_{frag}) for dissociation in accordance with eq 1: 116.6/172.4, 138.3/197.2, 150.4/212.5, and 153.3/217.7 kJ mol^{-1} (where E_{frag} refers to dissociation into fragments frozen so as to retain the geometries they assume in the adduct). The E_{diss} values are in satisfactory agreement with experimental[20] and earlier theoretical[22] estimates, while the E_{frag} values imply that the total relaxation energies for the isolated dissociation fragments increase somewhat across the series, viz. from 55.8 to 64.4 kJ mol^{-1}.

3.2. Crystal Structures of 1−3. Salient interatomic distances and interbond angles derived from the crystal structures determined by X-ray diffraction for single crystals of the adducts **1**−**3** are listed in Table 6. Before discussing these structures, however, we note that ammonia−borane, $H_3N\cdot BH_3$, forms monoclinic crystals in which the molecules pack in layers wherein a given molecule is surrounded by six others (see Figure 5i).[10,11] The most striking feature about the intermolecular contacts is the development of short N−H···H−B 'dihydrogen' bonds within the layers with H···H distances measuring 1.97 and 2.19 Å(labeled 'B' in Figure 5i); between the layers (Figure 5ii) there is weaker binding that appears again to involve N−H···H−B interactions, now with H···H distances of 2.24

(63) Jagielska, A.; Moszyński, R.; Piela, L. *J. Chem. Phys.* **1999**, *110*, 947.

(64) Demaison, J.; Liévin, J.; Császár, A. G.; Gutle, C. *J. Phys. Chem. A* **2008**, *112*, 4477.

Table 6. Distances (Å) and Interbond Angles (deg) of the $Me_nH_{3-n}N{\bullet}BH_3$ Molecules ($n = 1-3$) in Crystalline **1**, **2**, and **3**, Respectively

1		Distances[a]	
B(1)−N(1)	1.5936(13)	B(1)−H(11)#1	1.134(9)
N(1)−C(2)	1.4750(13)	B(1)−H(21)	1.121(13)
N(1)−H(1)	0.881(9)	C(2)−H(12)	0.959(12)
N(1)−H(1)#1	0.881(9)	C(2)−H(12)#1	0.959(12)
B(1)−H(11)	1.134(9)	C(2)−H(22)	0.971(14)
		Angles[a]	
B(1)−N(1)−C(2)	114.52(8)	N(1)−B(1)−H(21)	107.8(7)
H(1)#1−N(1)−B(1)	109.5(6)	H(11)#1−B(1)−H(21)	111.6(6)
H(1)#1−N(1)−C(2)	108.3(6)	H(11)−B(1)−H(21)	111.6(6)
H(1)#1−N(1)−H(1)	106.2(12)	N(1)−C(2)−H(12)#1	108.0(6)
B(1)−N(1)−H(1)	109.5(6)	N(1)−C(2)−H(12)	108.0(6)
C(2)−N(1)−H(1)	108.3(6)	H(12)#1−C(2)−H(12)	111.0(14)
N(1)−B(1)−H(11)#1	107.8(5)	N(1)−C(2)−H(22)	109.9(8)
N(1)−B(1)−H(11)	107.8(5)	H(12)#1−C(2)−H(22)	109.9(8)
H(11)#1−B(1)−H(11)	110.2(9)	H(12)−C(2)−H(22)	109.9(8)
2		Distances[a]	
B(1)−N(1)	1.5965(13)	C(2)−H(12)	0.969(12)
N(1)−C(2)	1.4734(13)	C(2)−H(22)	1.006(12)
N(1)−C(3)	1.4731(14)	C(2)−H(32)	0.973(13)
N(1)−H(1)	0.878(11)	C(3)−H(13)	0.989(12)
B(1)−H(11)	1.118(6)	C(3)−H(23)	0.977(12)
B(1)−H(21)	1.129(6)	C(3)−H(33)	0.982(12)
B(1)−H(31)	1.125(6)		
		Angles[a]	
B(1)−N(1)−C(2)	112.03(8)	N(1)−C(2)−H(12)	108.8(8)
B(1)−N(1)−C(3)	112.71(8)	N(1)−C(2)−H(22)	106.9(7)
C(2)−N(1)−C(3)	110.37(9)	H(12)−C(2)−H(22)	110.0(10)
B(1)−N(1)−H(1)	107.0(7)	N(1)−C(2)−H(32)	108.7(8)
C(2)−N(1)−H(1)	106.4(7)	H(12)−C(2)−H(32)	110.8(10)
C(3)−N(1)−H(1)	108.0(7)	H(22)−C(2)−H(32)	111.4(10)
N(1)−B(1)−H(11)	107.21(6)	N(1)−C(3)−H(13)	110.2(8)
N(1)−B(1)−H(21)	107.21(6)	N(1)−C(3)−H(23)	108.4(8)
H(11)−B(1)−H(21)	111.62(6)	H(13)−C(3)−H(23)	110.9(10)
N(1)−B(1)−H(31)	107.23(6)	N(1)−C(3)−H(33)	108.1(8)
H(11)−B(1)−H(31)	111.64(6)	H(13)−C(3)−H(33)	110.7(10)
H(21)−B(1)−H(31)	111.63(6)	H(23)−C(3)−H(33)	108.5(10)
3		Distances[a]	
B(1)#2−N(1)	1.617(4)	C(1)−H(21)	0.979(9)
N(1)−C(1)	1.4825(16)	C(1)−H(21)#3	0.979(9)
N(1)−C(1)#1	1.4832(16)	B(1)−H(1)	1.16(3)
N(1)−C(1)#2	1.4832(16)	B(1)−H(1)#1	1.16(3)
C(1)−H(11)	0.984(9)	B(1)−H(1)#2	1.16(3)
		Angles[a]	
B(1)#2−N(1)−C(1)	110.53(9)	N(1)#4−C(1)−H(21)	109.3(10)
B(1)#2−N(1)−C(1)#1	110.49(9)	N(1)−C(1)−H(21)	109.3(10)
B(1)#2−N(1)−C(1)#2	110.46(9)	H(21)#3−C(1)−H(21)	105(2)
C(1)#1−N(1)−C(1)#2	108.40(9)	H(11)−C(1)−H(21)	111.9(14)
C(1)#1−N(1)−C(1)	108.44(9)	N(1)#4−B(1)−H(1)#1	106.4(20)
C(1)#2−N(1)−C(1)	108.44(9)	N(1)#4−B(1)−H(1)#2	106.5(20)
N(1)#4−C(1)−H(21)#3	109.3(10)	H(1)#1−B(1)−H(1)#2	112.3(17)
N(1)−C(1)−H(21)#3	109.3(10)	N(1)#4−B(1)−H(1)	106.5(20)
N(1)#4−C(1)−H(11)	109.3(16)	H(1)#1−B(1)−H(1)	112.3(17)
N(1)−C(1)−H(11)	109.3(16)	H(1)#2−B(1)−H(1)	112.3(17)
H(21)#3−C(1)−H(11)	111.9(14)		

[a] See Figure S3 in the Supporting Information for atom labeling. For compound **1** #1 denotes $x, -y + 1/2, z$; for compound **3** #1 denotes $-x + y, -x + 1, z$, #2 denotes $-y + 1, x - y + 1, z$, #3 denotes $-y + 1, -x + 1, z$, and #4 denotes $-x + y, y, z$.

Å (labeled 'C'). Distances involving hydrogen atoms are calculated here and elsewhere in this section after 'normalization' of C−H, N−H, and B−H distances to typical neutron values (1.083, 1.009, and 1.190 Å, respectively).[52]

By contrast, methylamine−borane **1** forms orthorhombic crystals in which the molecules of the adduct are linked in ribbons running along the *b* axis (Figure 6i). Within the ribbons successive molecules are aligned with the B−N bonds directed along the *c* axis and antiparallel to one another; each pair of molecules is related by an inversion center and linked by two

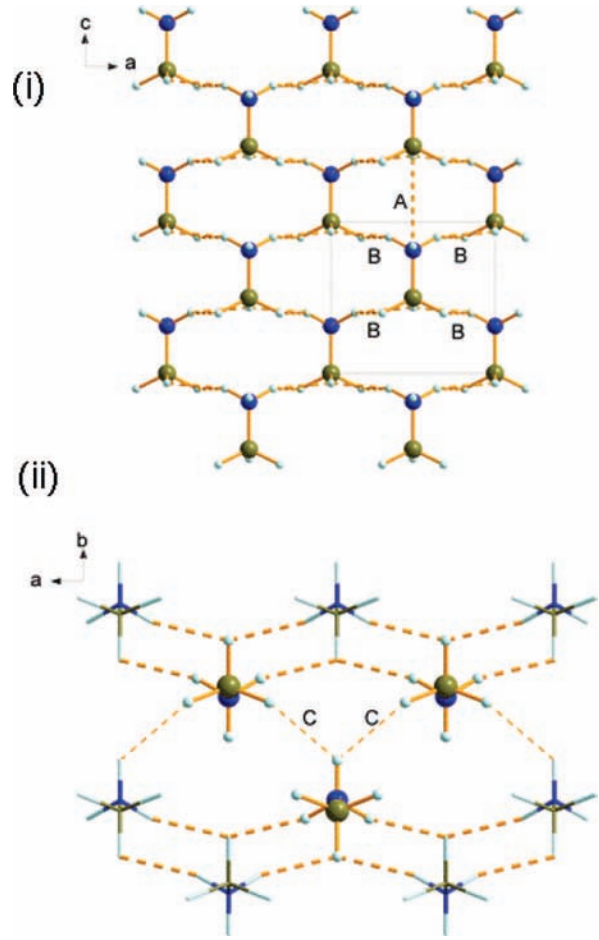

Figure 5. (i) Layers formed through H···H contacts in $H_3N{\cdot}BH_3$. The molecules lie on *m*.. sites. The labels A and B refer to the intermolecular contacts listed as A_0 and B_0 in Table 8. (ii) The crystal structure of $H_3N{\cdot}BH_3$ viewed along *c*. Only H···H contacts less than 2 Å are shown in order to emphasize the layers. The highlighted molecule in the lower layer makes contacts (C_0 in Table 8) to the highlighted molecules in the layer above. Color scheme: N, blue; H, white; B, brown.

Table 7. Comparison of Total Lattice Energies, E_{TOTAL}, Calculated by SCDS-PIXEL Methods for the Crystalline Adducts $Me_nH_{3-n}N{\bullet}BH_3$ with the Experimental Sublimation Enthalpies, $\Delta_{sub}H_m$, and Earlier Theoretical Estimates[a]

adduct	E_{TOTAL}[b]	$\Delta_{sub}H_m$(exp)	other estimates
$H_3N{\cdot}BH_3$	−101.0	−97.0[c]	$E_{TOTAL} = -79.2$[d] $\Delta_{sub}H^\circ = -88.0$[c]
$MeH_2N{\cdot}BH_3$	−93.3	−78.7(42)[e]	
$Me_2HN{\cdot}BH_3$	−85.0	−77.4(29)[e]	
$Me_3N{\cdot}BH_3$	−65.0	−56.9(8)[e]	

[a] All energies are in kJ mol^{-1}. [b] This work. [c] See ref 66, Table 1. [d] Result of plane-wave density functional theory calculations, see ref 15. [e] See ref 23c.

H···H contacts (labeled 'A') measuring 2.00 Å. The ribbons are in turn linked into a layer via H···H contacts ('B' in Figure 6ii) of 2.42 Å, and still weaker N−H···H−C interactions (at 2.89 Å, 'C') contribute to the forces holding the layers together.

The monoclinic crystals formed by dimethylamine−borane **2** find the adduct molecules building up chains that run along the *b* axis (Figure 7i). Again H···H bonding is much in evidence in linking the molecules head-to-tail, this time featuring as a bifurcated BH_2···HN interaction with H···H distances of 1.95 and 2.08 Å (labeled 'B'). Each chain is surrounded by neighboring chains (Figure 7ii) experiencing relatively close

Table 8. Intermolecular Interaction Energies (kJ mol^{-1}) Derived from SCDS-PIXEL Calculations for $H_3N \cdot BH_3$, $MeH_2N \cdot BH_3$, $Me_2HN \cdot BH_3$, and $Me_3N \cdot BH_3$[a]

adduct	interaction	Coulombic	polarization	dispersion	repulsion	total	notes
$H_3N \cdot BH_3$	A_0	−28.6	−4.9	−7.9	+6.0	−35.4	2 intralayer head-to-tail Coulombic contacts
	B_0	−12.3	−16.1	−12.3	+22.1	−18.6	4 intralayer contacts H···H 1.97 Å H···H 2.19 Å
	C_0	−0.4	−4.3	−5.4	+5.1	−5.0	4 interlayer contacts H···H 2.24 Å
1	A_1	−62.2	−24.3	−22.2	+37.9	−70.7	2 ribbon-forming contacts H···H 2.00 Å
	B_1	−26.7	−6.9	−12.7	+12.8	−33.5	2 contacts linking ribbons into a layer H···H 2.42 Å
	C_1	−7.4	−1.2	−3.2	+1.3	−10.5	2 contacts linking the layers C−H···H−B 2.89 Å
2	A_2	−19.4	−3.9	−11.6	+8.7	−26.2	1 interchain interaction across an inversion center
	B_2	−22.0	−18.8	−17.5	+33.8	−24.5	2 chain-forming contacts H···H = 1.95 and 2.08 Å
	C_2	−18.5	−4.1	−9.5	+8.8	−23.4	2 next-nearest neighbor interactions with chain
	D_2	−16.8	−3.2	−8.3	+8.0	−20.3	1 interchain interaction across an inversion center
	E_2	−4.1	−0.9	−3.8	+1.5	−7.3	2 interchain interactions
3	A_3	−17.5	−4.8	−13.2	+11.4	−24.2	2 head-to-tail chain-building contacts C−H···H−B = 2.66 Å
	B_3	−1.9	−1.2	−4.7	+2.4	−5.4	6 contacts in $z = -2/3$ and $+2/3$ layers
	C_3	+4.0	−2.0	−10.8	+5.9	−2.9	6 contacts in $z = -1/3$ and $+1/3$ layers

[a] H···H distances calculated with normalized H-atom positions. On the basis of the data presented in Figure 9, the numerical values are likely to be slight overestimates.

interchain contacts ('A', 'D', and 'E'). The shortest H···H distances in each of these contacts and their inversion-related symmetry-equivalents are H21···H33, 2.38 Å; H23···H11, 2.42 Å; and H32···H12, 2.55 Å.

Trimethylamine−borane **3** forms rhombohedral crystals in which the molecular coordination number of each molecule is 14, the structure being topologically similar to body-centered cubic packing. Head-to-tail interactions between the Me_3N and BH_3 groups link the molecules in chains along the *c* axis (Figure 8) with shortest C−H···H−B contacts of 2.66 Å.

Irrespective of the mode of aggregation, none of the methylamine−borane molecules suffers any radical change on crystallization. Due allowance must be made for the different estimates of interatomic distance (commonly amounting to about 0.1 Å for bonds in which hydrogen is engaged) made on the basis of electron or neutron diffraction on the one hand and of X-ray diffraction on the other. It then appears that the molecules invariably maintain a staggered conformation about the B−N bond and that there is no significant change in the internal bond lengths of the amine and borane moieties on crystallization. In only two respects can a meaningful change be found between the intramolecular dimensions of the adduct molecules, as they appear in the gaseous and crystalline phases. First, with B−N distances of 1.594(2), 1.597(2), and 1.617(4) Å in crystalline **1**, **2**, and **3**, respectively, the coordinate link is observed consistently to contract (by 0.036−0.047 Å) with the switch from the gaseous to the solid phase. In this respect, the adducts follow the example of not only ammonia−borane,[10,11] but also other adducts featuring a coordinate link between a Group 13 acceptor and a nitrogen base, e.g., $Me_3N \cdot GaH_3$.[65] Despite the energetic cost, compression of the polar coordinate link leads to an increased dipole moment for the adduct molecule, giving rise in turn to heightened Coulombic interactions, irrespective of any other factors governing the crystal packing. Simultaneously with the shortening of the B−N distance, the BH_3 pyramid acquires an even sharper pitch, with the sum of the three H−B−H angles decreasing by a further 3.3−6.2°. There appears also to be a corresponding tightening of the interbond angles at nitrogen (the sum decreasing by 2−3°) in the $Me_nH_{3-n}N$ fragment (see Table 6).

3.3. Analysis of the Intermolecular Interactions in the Crystals: Results of SCDS-PIXEL Calculations. The SCDS-PIXEL method has been developed recently by Gavezzotti for analysis of intermolecular interaction energies.[28a−c,51] Its performance in reproducing experimental sublimation enthalpies for a range of organic compounds has been examined in ref 28c. In a comparison of 91 organic compounds, PIXEL lattice energies (*y*) were found to be related to experimental sublimation energies (*x*) by the straight line relationship $y = 1.03x$ with a correlation coefficient equal to 0.92.[28d] For hydrogen-bonded dimers, PIXEL results were found to be in very good agreement with other theoretical and experimental estimates of binding energies: for the water dimer, for example, the experimental and PIXEL binding energies are 22.6 and 23 kJ mol^{-1}, respectively.[28d] Periodic DFT and PIXEL results have been found to agree on changes which occur in the lattice energy of serine as a function of pressure.[28e] The PIXEL method also reproduces the lattice energy of benzene, performing rather better than a number of commonly applied theoretical models;[28e] on the other hand, interactions between benzene and polar molecules such as ammonia and water are less well modeled.[28d]

As a test of the reliability of SCDS-PIXEL calculations for boron compounds, we begin by comparing the total lattice energy calculated for each of the crystalline adducts $Me_nH_{3-n}N \cdot BH_3$ ($n = 0-3$) with values from other sources,[15,66] including, particularly, experimental estimates of the sublimation energy.[23c] The calculations have also been extended to the six other boron-containing compounds noted earlier.

The results are depicted in Figure 9, with more detailed information on the adducts set out in Table 7. While the PIXEL procedure tends to *over*estimate lattice energies of boron compounds on average by about 10%, for $H_3N \cdot BH_3$ they improve on earlier theoretical calculations involving plane-wave density functional theory.[15] Among the adducts, the largest discrepancy is found in the case of **1**.[23c] This may reflect weaknesses in the SCDS-PIXEL approach: sources of error are (a) the assumption that electron density distributions are undistorted in the solid state, (b) the assumed corrections from X-ray to neutron bond distances involving hydrogen, (c) the

(65) See, for example, the following: (a) Brain, P. T.; Brown, H. E.; Downs, A. J.; Greene, T. M.; Johnsen, E.; Parsons, S.; Rankin, D. W. H.; Smart, B. A.; Tang, C. Y. *J. Chem. Soc., Dalton Trans.* **1998**, 3685. (b) Marchant, S.; Tang, C. Y.; Downs, A. J.; Greene, T. M.; Himmel, H.-J.; Parsons, S. *Dalton Trans.* **2005**, 3281. (c) Wann, D. A.; Blockhuys, F.; Van Alsenoy, C.; Robertson, H. E.; Himmel, H.-J.; Tang, C. Y.; Cowley, A. R.; Downs, A. J.; Rankin, D. W. H. *Dalton Trans.* **2007**, 1687.

(66) Matus, M. H.; Anderson, K. D.; Camaioni, D. M.; Autrey, S. T.; Dixon, D. A. *J. Phys. Chem. A* **2007**, *111*, 4411.

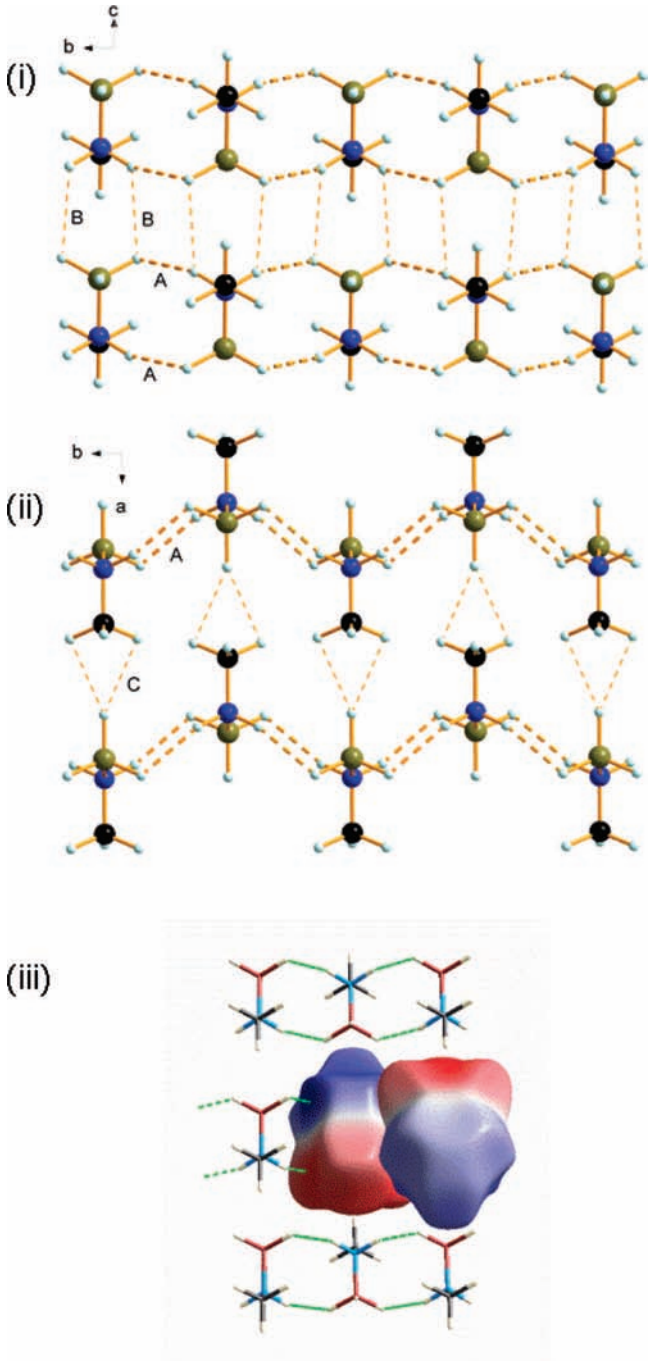

Figure 6. Formation of layers in the crystal structure of **1** as viewed (i) along *a* and (ii) along *c*. The labels A−C refer to the intermolecular contacts A_1−C_1 listed in Table 8. (iii) Packing in the layers in **1** with some molecules shown with Hirshfeld surfaces encoded with the electrostatic potential mapped over the range −0.1 au (red) to +0.1 au (blue). The same range is used in Figures 7 and 8.

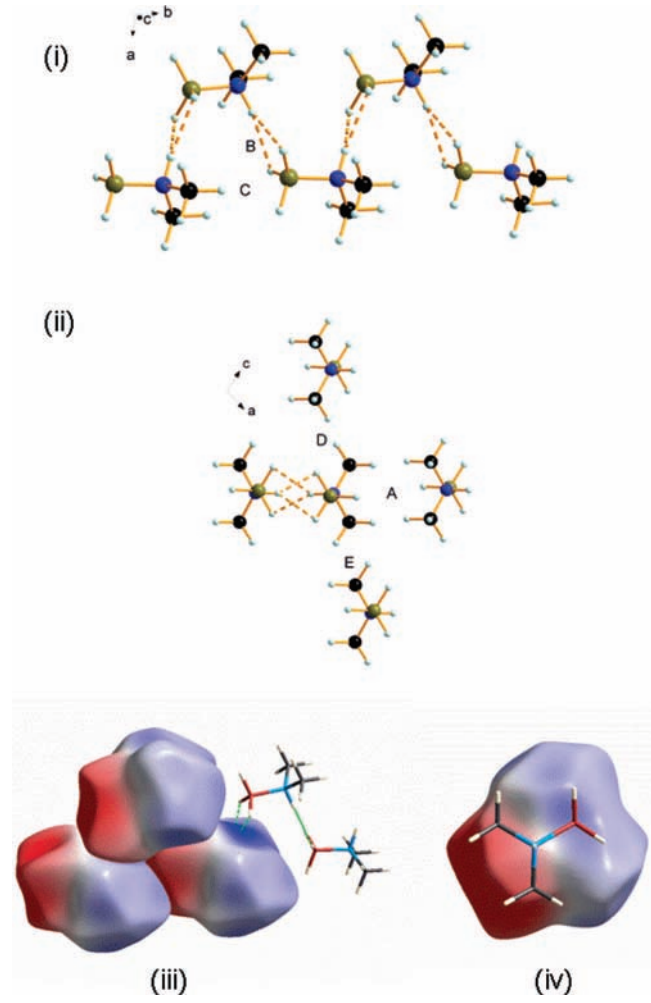

Figure 7. (i) Chains formed by H···H (contact B_2 in Table 8) and electrostatic interactions (C_2) in the crystal structure of **2**. (ii) The most significant interchain interactions (A_2, D_2, and E_2 in Table 8). (iii) Chains shown in (i) with the molecules having Hirshfeld surfaces encoded with the electrostatic potential; note the close disposition of the positive (blue) and negative (red) regions. (iv) The Coulombic term in interchain interaction A_2 illustrated using ESP-encoded Hirshfeld surfaces. Only one contacting surface is shown, the other being generated by an inversion center between the molecules.

neglect of zero-point energy and thermal corrections, and (d) neglect of intramolecular conformational changes which occur on sublimation. However, the reliability of the experimental value is also open to doubt, particularly as the vapor pressure plot for **1** shows a significantly greater degree of scatter in this case,[23b] and the vapor pressure equation derived may well give undue weight to a single, isolated point at low temperature (ca. 280 K). Still more doubt is raised by the findings of our GED experiments, which indicate that the vapor of **1** at ca. 360 K, unlike that of **2**, witnesses a significant degree of dissociation of the **1** molecules (see Section 3.1). We cannot be sure of course, but experiment, in the shape of the earlier vapor pressure measurements, may err at least as grossly as theory. Indeed, different *experimental* determinations of sublimation enthalpies can differ substantially even in the cases of well-behaved compounds: for example, the values quoted in ref 23c for BPh_3 are 103.8 ± 2.5, 92.1 ± 2.5, and 81.6 ± 2.1 kJ mol^{-1}.

While there is a systematic error in the absolute values of the PIXEL lattice energies, the correlation coefficient between the data shown in Figure 9 is 0.95, meaning that the PIXEL method calculates *trends* in intermolecular energies very accurately. We feel therefore that this initial test justifies our proceeding to use the results of the calculations to analyze the details and energetics of molecular packing in crystals of the $Me_nH_{3-n}N\cdot BH_3$ adducts. The energy values quoted below are likely to be upper limits, numerically too large by perhaps 10%.

3.3.1. $H_3N\cdot BH_3$. The three most significant contacts, A_0−C_0, are listed in Table 8; in addition, there are 14 contacts with energies between −5 and +14 kJ mol^{-1} that are long-range attractive and repulsive Coulombic interactions. Interactions A_0

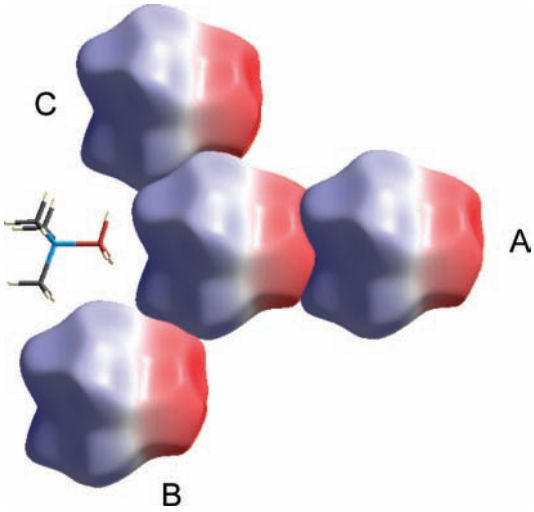

Figure 8. Head-to-tail arrangement of molecules in crystalline **3** forms chains running along the *c* direction (here horizontal). This is interaction A_3 in Table 8. Neighboring chains interact through contacts B_3 and C_3, the latter being weaker. The molecules are shown with Hirshfeld surfaces encoded with the electrostatic potential; notice the larger blue−blue contact in interactions of type C.

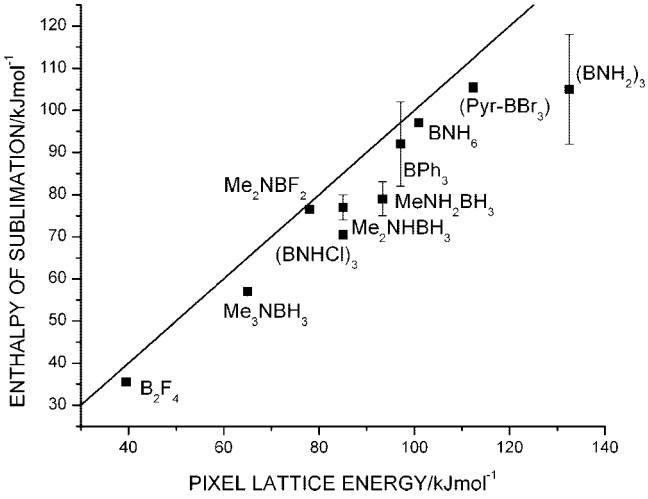

Figure 9. Comparison of experimental enthalpies of sublimation with total lattice energies calculated using the PIXEL procedure for a variety of boron-containing compounds. The line represents the function $y = x$; error bars are drawn where experimental estimates of precision are available.

and B_0 occur within the layers in which the molecules pack (Figure 5i). Intermolecular interaction B_0 features dihydrogen bonds. While the energies of 'conventional' hydrogen bonds are usually dominated by the electrostatic term, the same is not true here, and both polarization and dispersion are important. The layers interact with layers above and below via weaker contacts C_0 (Figure 5ii). The shortest H···H distances formed between the layers are only slightly longer than some of those within the layers, but the difference in energies is quite marked (19 vs 5 kJ mol^{-1}). Interactions A_0, B_0, and C_0 account for about 77% of the lattice energy of $H_3N \cdot BH_3$; the remaining energy arises from numerous longer range electrostatic interactions between zwitterions.

Some insight into the packing can be gained from a Hirshfeld surface plot colored to show the electrostatic potential, as

Table 9. Dihydrogen Bond Energies (kJ mol^{-1}) Estimated for $H_3N \cdot BH_3$, **1**, and **2** on the Basis of SCDS-PIXEL Calculations[a]

adduct	E_{TOTAL}	H···H distance (Å)	contact	notes[b]
$H_3N \cdot BH_3$	−18.6	1.97, 2.19	B_0	breakdown: $E_C = -12.3$ $E_P = -16.1$ $E_D = -12.3$ $E_R = +22.1$
	−5.0	2.24	C_0	
1	−70.7	2.00	A_1	breakdown: $E_C = -62.2$ $E_P = -24.3$ $E_D = -22.2$ $E_R = +37.9$
2	−24.5	1.95, 2.08	B_2	breakdown: $E_C = -22.0$ $E_P = -18.8$ $E_D = -17.5$ $E_R = +33.8$

[a] H···H distances calculated with normalized H-atom positions. [b] Subscript abbreviations: C = Coulombic, P = polarization, D = dispersion, and R = repulsion.

recently described by McKinnon et al.[67] $H_3N \cdot BH_3$ is essentially a cylindrical molecule with positively and negatively charged ends. The pseudo-body-centered cubic packing established by contacts B_0−E_0 is readily understood in terms of optimization of contacts between positive and negative ends of the molecules.

3.3.2. $MeH_2N \cdot BH_3$ (1). Again, there are three principal types of intermolecular contact, A_1−C_1, with the calculated energies listed in Table 8. Interaction A_1 involves a pair of molecules, related by an inversion center, linked by two H···H contacts (at 2.00 Å, see Figure 6i). Successive inversion centers link the molecules into the ribbon running along the *b* axis. This contact is very strong - much stronger than any contact in $H_3N \cdot BH_3$; it incorporates two H···H bonds and antialigns the dipoles of the molecules. Contact B_1 links the ribbons into a layer in the *bc* plane. The shortest H···H distance between the molecules involved in this contact is 2.42 Å; the interaction is rather similar to contact A_0 in $H_3N \cdot BH_3$ (where the shortest H···H distance is 2.56 Å), except that the dispersion component is bigger. Interaction C_1 links the layers. Now the shortest H···H contact, measuring 2.89 Å, is formed between a methyl H atom and an H atom of a BH_3 group (Figure 6ii). The energy is quite modest and mostly electrostatic in origin. The interlayer stacking appears to be mediated by methyl groups and the interactions are therefore quite weak. This feature can also be illustrated by inspection of a Hirshfeld plot of electrostatic potential (Figure 6iii); all the most 'electrostatically active' (i.e., most intensely colored) parts of the surface are oriented within the layers.

In addition to the contacts listed in Table 8, there are numerous longer range Coulombic interactions. These are both attractive and repulsive, and span the energy range from −8 to +8 kJ mol^{-1}.

3.3.3. $Me_2HN \cdot BH_3$ (2). Of the main intermolecular contacts in crystalline **2** listed in Table 8, four (A_2−D_2) have energies between −20 and −30 kJ mol^{-1}, while the fifth (E_2) has a substantially lower energy at −7.3 kJ mol^{-1}; the energy of the next strongest contact is −3.9 kJ mol^{-1}. Interactions B_2 and C_2 build up the chain running along the *b* axis (Figure 7i). B_2 comprises the two H···H contacts measuring 1.95 and 2.08 Å and in which the dispersion and polarization components are almost as energetic as the Coulombic term. Next-nearest

(67) Spackman, M. A.; McKinnon, J. J.; Jayatilaka, D. *CrystEngComm* **2008**, *10*, 377.

Table 10. Comparison of Total Intermolecular Energy Terms (kJ mol^{-1}) in Dimer Interactions Featuring Dihydrogen Bonds and in Some Representative Conventional Hydrogen Bonds[a]

interaction	type	E_C	E_P	E_D	E_R	E_{TOTAL}
benzoic acid dimer[b]	O−H···O=C	−43	−17	−8	+33	−36
benzamide dimer[b]	N−H···O=C	−38	−16	−10	+40	−23
phenol dimer[b]	O−H···O−H	−41	−18	−14	+50	−22
$H_3N{\cdot}BH_3$[c]	N−H···H−B	−12	−16	−12	+22	−19

[a] Subscript abbreviations: C = Coulombic, P = polarization, D = dispersion, and R = repulsion. [b] See ref 28b. [c] This work.

neighbors in the chain are related by lattice translations along *b*, and take the form of head-to-tail arrangement of **2** molecules with an electrostatic interaction between successive amine and borane groups. The electrostatic potential plotted in Figure 7iii shows this clearly.

Each chain is surrounded by six neighboring chains, the four most energetic interactions being shown in Figure 7ii. One of the interchain contacts (A_2) is the strongest intermolecular interaction in the crystal, being a mixture of Coulombic and dispersion terms. The Coulombic part arises from contacts between the positively charged methyl H and the negatively charged borane H atoms (Figure 7iv). Similar comments apply to interactions D_2 and E_2, but the contact surface area is smaller, and this may explain why they are weaker contacts.

3.3.4. $Me_3N{\cdot}BH_3$ (3). The most significant intermolecular contacts in crystalline **3** number three (A_3−C_3); their properties are as listed in Table 8. A_3 involves two contacts, while B_3 and C_3 involve six contacts each. The A-type contacts are formed through head-to-tail interactions between the amine and borane groups, giving rise to the chain along the *c* axis (Figure 8). The 12 contacts corresponding to interactions B_3 and C_3 surround the chains along this axis, with energies dominated by dispersion terms. Interaction C_3 is actually slightly repulsive in its Coulombic term, a feature that is understandable in the contacts between the blue regions of the middle and top surfaces of electrostatic potential shown in Figure 8.

3.4. Dihydrogen Bond Energies. The energies of the major N−H···H−B interactions that might reasonably be regarded as incorporating dihydrogen bonds in the adducts $Me_nH_{3-n}N{\cdot}BH_3$ are listed in Table 9. The PIXEL calculations evaluate molecule−molecule interaction energies. Single, strong H···H interactions are a feature of the crystal structures of both $H_3N{\cdot}BH_3$ and **1**. The shortest H···H contacts in crystalline **1**, linking the molecules in pairs, are noteworthy for the very strong electrostatic contribution involved. By contrast, the shortest H···H contact in crystalline **2** relates to a bifurcated dihydrogen bond and is therefore rather different from the others. Perhaps the most nearly comparable H···H contacts are those in $H_3N{\cdot}BH_3$ and **1**. The latter gives a stronger dihydrogen bond, with a larger electrostatic term. Consideration of the inductive effect of the methyl group might have been expected to lead to a *smaller* term, the ab initio population analysis placing charges of +0.37e and +0.26e on the amine H atoms in $H_3N{\cdot}BH_3$ and **1**, respectively. The explanation for this apparent anomaly is not obvious, although it should be appreciated that there is more to each of the interactions than just the dihydrogen bonds. For example, the very strong interaction in **1** features a closely, antialigned pair of very polar molecules linked by two H···H contacts.

Finally, Table 10 lists for comparison the intermolecular contact energies mediated by dihydrogen bonds in $H_3N{\cdot}BH_3$ with those of some representative 'conventional' hydrogen bonds. The dihydrogen bond energy in $H_3N{\cdot}BH_3$ has been previously estimated to be 12.7 kJ mol^{-1} in ref 15 and 15 kJ mol^{-1} in ref 66. The value obtained using the PIXEL method (−19 kJ mol^{-1}, Table 10) is a little higher than these. That this should be the case is not surprising given the tendency of the PIXEL method (with its present parametrization) to overestimate sublimation enthalpies for boron compounds (Figure 9); on balance, our value might be considered an upper limit for the H···H interaction energy in $H_3N{\cdot}BH_3$.

On the evidence of the data in Table 10, dihydrogen bonds have polarization and dispersion energies that are similar to those in conventional hydrogen bonds but smaller Coulombic energies. The greater relative importance of the polarization and dispersion terms appears therefore to distinguish dihydrogen from more conventional hydrogen bonds. Overall, however, the intermolecular interaction energies evaluated here are toward the low end of the range associated with hydrogen bonds of medium strength, a conclusion in agreement with that reached by Morrison and Siddick in ref 15.

Conclusions

In an effort to gain the fullest possible understanding of the structural properties of borane adducts of the type $Me_nH_{3-n}N{\cdot}BH_3$ for $n = 0$−3 in the gaseous and crystalline phases, we have determined the structures of the molecules **1** and **2** by GED, with restraints supplied by appropriate quantum chemical calculations. In addition, we have employed X-ray diffraction to determine the crystal structures of **1**, **2**, and **3**. The GED studies of **1** were complicated by partial dissociation of the adduct into MeH_2N and B_2H_6, but structures consistent with the results of high-level ab initio calculations have now been determined for all the gaseous molecules in this series. Despite a 23% increase in the experimentally estimated dissociation energy on passing from $H_3N{\cdot}BH_3$ to **3**, the geometries of the adduct molecules reveal only slight changes with progressive methylation at the nitrogen center. Thus, the B−N bond length varies but little for the methylamine−boranes, while increasing slightly (by about 0.02 Å) in $H_3N{\cdot}BH_3$. There are also minor changes in the angles subtended by the bonds to the substituents at the B and N centers, with the $C_nH_{3-n}N$ moiety tending to become slightly less pyramidal and the BH_3 one slightly more pyramidal as *n* increases.

The crystallographic studies show that all the adducts form crystals in which the $Me_nH_{3-n}N{\cdot}BH_3$ molecules do not deviate greatly from the structures they assume in the gas phase. Crystallization causes a shortening of the B−N link by about 0.094 Å for $H_3N{\cdot}BH_3$ [9−11] and 0.036−0.047 Å for the methylamine−boranes, while there is also some tightening of the interbond angles made by the substituents at B and N. Where $H_3N{\cdot}BH_3$ has already been shown to form crystals in which the adduct molecules pack in layers, the methylamine-boranes, **1**−**3**, all form crystals in which the molecules are linked in chains. In common with $H_3N{\cdot}BH_3$, both **1** and **2** reveal evidence of significant intermolecular N−H···H−B 'dihydrogen' bonds with short H···H contacts measuring about 2.0 Å. The relative importance of these and other secondary interactions has been assessed for all the members of the series by carrying out SCDS-PIXEL calculations.[28] Hence, we conclude that dihydrogen bonds resemble conventional hydrogen bonds in their polarization and dispersion energies but differ from them in having distinctly smaller Coulombic energies. Nevertheless, the total intermolecular interaction energies evaluated for dihydrogen bonds in $H_3N{\cdot}BH_3$ and the methylamine−boranes are compa-

rable overall with those of such conventional hydrogen bonds as are found, for example, in solid phenol.

Acknowledgment. We thank the EPSRC for funding the electron-diffraction research (Grant No. EP/C513649) and for postdoctoral funding of C.Y.T. (Grant No. EP/F01600X). We are grateful also to Prof. Angelo Gavezzotti for a copy of the program OPiX for the PIXEL calculations, as well as much helpful advice.

Supporting Information Available: Complete ref 42 available. Details of the GED experiments; treatment of the partial dissociation of gaseous **1**; models used in the GED refinements of **1** and **2**; interatomic distances, refined and calculated amplitudes of vibration and perpendicular corrections for the SARACEN-restrained GED structures of **1** and **2**; least-squares correlation matrices for the refined GED structures of **1** and **2**; GED and calculated coordinates for **1** + its dissociation products and for **2**; molecular scattering intensity and difference curves for the GED refinements of **1** + its dissociation products and of **2** (Figures S1 and S2). Atom numbering used for the crystal structures of **1**−**3** (Figure S3). CIF files for the crystal structures of **1**−**3**. This material is available free of charge via the Internet at http://pubs.acs.org.

JA807545P